Hindawi
International Journal of Aerospace Engineering
Volume 2020, Article ID 5313941, 13 pages
https://doi.org/10.1155/2020/5313941

Research Article

Study on Inlet and Engine Integrated Model with Normal Shock Position Feedback

Haoying Chen, Haibo Zhang, Zhihua Xi, and Qiangang Zheng

Jiangsu Province Key Laboratory of Aerospace Power System, College of Energy and Power Engineering, Nanjing University of Aeronautics and Astronautics, No. 29 Yudao Street, Nanjing 210016, China

Correspondence should be addressed to Haibo Zhang; zh_zhhb@126.com

Received 27 July 2019; Revised 11 October 2019; Accepted 18 December 2019; Published 4 January 2020

Academic Editor: Paul Williams

In order to consider the inlet and engine integrated model of supersonic airliner, the dynamic identification and control of inlet normal shock are studied. The research is based on the bleed air flow rate under supersonic conditions. With the two-dimensional CFD model of supersonic inlet, the dynamic and static effects of the bleeding flow rate on the normal shock position were investigated. The transfer function was identified, and simultaneously the paper carried out a comprehensive study of inlet and engine integrated model, which is established based on the inlet shock position model and engine component level model. The relationship between normal shock position and total pressure recovery coefficient has been taken into consideration in this model. Based on the inlet and engine integrated model, the closed-loop control simulation of normal shock position is carried out. The results show that the model could resist the disturbance of the inlet flow and keep the inlet and engine matching operation point stable near the optimal value.

1. Introduction

The aircraft may encounter various disturbances in flight, such as the atmospheric turbulence, the shock waves of passing through another aircraft, and the pulsation of engine airflow, which would affect the inlet operation. If these methods of increasing the stability and safety margin are taken into account in the process of inlet design, the inlet performance would deteriorate under normal conditions [1, 2]. The purpose of inlet control is to avoid the inlet or engine surge when entering the strong subcritical or supercritical state after disturbance. Meanwhile, the control makes the engine return to approximate optimal working state quickly. However, it is impossible to maintain the propulsion system in the best performance state by manipulating the bleed valve, which keeps the normal shock position unchanged. For example, in order to adapt the disturbance, the inlet may increase the bleed flow leading to the bleed drag, which is shown in Figure 1. (C_{bp} is the coefficient of bleed drag, A_{bleed} is the bleed area, and A_c is the inlet capture area.) Therefore, even if the shock wave remains at a position of high-pressure recovery coefficient, it may still cause a net loss of the propulsion system [3, 4]. Because the pressure of fan inlet has influence on the normal shock wave position, it may be better to adopt the integrated adjustment of the bleed valve and engine to control the position.

The engine control mechanism must meet the requirements of a minimum noise level and optimal economy in thrust control. Meanwhile, the engine rotor speed and turbine inlet temperature could not exceed limit in order to ensure the stability of fan, compressor, and combustion chamber. The engine used in supersonic passenger aircraft can be divided into the following: main operating conditions, engine start-up, take-off, acceleration and climbing, the subsonic flight whose airline is set in residential areas, supersonic cruise, and landing [5–7]. Corresponding to the different working conditions, the control tasks are different. During the flight supersonic cruise, it is necessary to ensure economy and give the best ride quality to the passengers, which

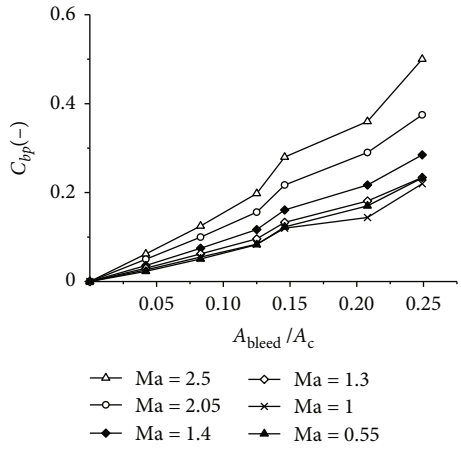

FIGURE 1: Relationship between inlet bleed drag coefficient and airflow.

requires the stable engine thrust and reduces the unnecessary flight attitude changes.

The research on supersonic inlet control has been developed continuously. The early aircrafts F-14 and F-18 used simple fixed baffle inlet; they then were developed into the advanced inlet whose swash plate or center cone could be adjusted [8]. For example, the Mirage 2000 has the semicircular center cone adjustable inlet; the F4 aircraft, Russian MiG-23s, and F-8 II have the rectangular inlet whose front swash plate is adjustable; and F-15 has the adjustable binary wedge-shape inlet. With the development of modern measurement and control technology, it is possible to capture normal shock or measure its position. The research of shock wave position detection and control has become a hot topic. Le et al. proposed three methods to monitor shock wave in isolation section of dual-mode scramjet, and the accuracy of three methods was compared by testing [9]. Hutzel et al. summarized the developing history of monitoring shock wave position and compared several monitoring schemes [10]. Donbar proposed a scramjet control method based on shock wave position [11]. When the aircraft is in high Mach number cruise, the upstream and downstream flow fields of the inlet are prone to fluctuate due to the drop of shock wave, the change of atmospheric environment, or the launch of weapon. It causes the change of inlet normal shock wave position and then affects the stability of inlet or even causes the engine surge [12–14].

In this paper, the research is focused on the integrated control of inlet and engine for supersonic airliner based on the control technology of normal shock wave position. This technology improves the anti-interference performance of the inlet and makes the inlet and engine operate at a better matching point. In the first section of this paper, the integrated model is established by the relationship between normal shock wave position and total pressure recovery coefficient. Subsequently, the integrated model is simulated to verify the antidisturbance ability of the closed-loop control. Finally, the inlet and engine integrated control model are established to reduce the influence of atmospheric disturbance to the propulsion system performance.

2. Inlet and Engine Integrated Model

In order to study the inlet and engine integrated control, the paper establishes an integrated model, which is a twin-bladed rotor, is mixed flow afterburner turbofan engine, and is shown in Figure 2. In the picture, the section numbers are as follows: section 2 is the exit of inlet, section 22 is the exit of fan, section 25 is the entrance of a high-pressure compressor, section 3 is the exit of a high-pressure compressor (HPC), section 4 is the exit of a combustor, section 45 is the exit of a high-pressure turbine, section 5 is the exit of a low-pressure turbine, section 6 is the mixing chamber, section 8 is the nozzle throat, section 9 is the exit of nozzle, section 13 is the entrance of the bypass, and section 16 is the exit of the bypass.

In this paper, the supersonic mixed pressure inlet is studied and the model is shown in Figure 3, where the section number 0 represents environment situation and 1 represents the entrance of the inlet. The design point of model is 2.2 Ma and 11 km (the static pressure is 22700 Pa, and static temperature is 216.7 K). The first, second, and third compression angle δ_1, δ_2, and δ_3 and the expansion section angle β are, respectively, 6 degrees.

The computational inlet model is shown in Figure 4. In order to simulate the operating process of the inlet accurately, a two-dimensional CFD calculation based on FLUENT software is carried out to simulate the dynamic changes of flow field under different flight conditions, up- and downstream disturbance, and bleeding regulation. The turbulence model based on FLUENT software adopts unsteady calculation. The time step is 0.01 ms, and the number of internal iteration steps is set to 30. The process of opening and closing the bleed valve is mainly realized by UDF (user-defined function) with dynamic grid technology, which is used to change the angle of the valve to adjust the bleed.

In order to facilitate the calculation, the following assumptions are set:

(1) The inlet air is the ideal gas that ignores the ionization effect of air

(2) The gravity and thermal radiation are not considered in the research

(3) The wall of the inlet is adiabatic

(4) The airflow inside and outside the two-dimensional supersonic inlet is two-dimensional compressible flow

When the shock wave position is disturbed, the position could remain unchanged by increasing or decreasing the bleed flow. In order to achieve high-quality bleed control regulation, the dynamic relationship between bleed and shock position should be obtained [15]. The transfer function between them ought to be further obtained by a two-dimensional CFD model. (Figure 5 shows the input curve of bleed flow and output curve of shock wave position.)

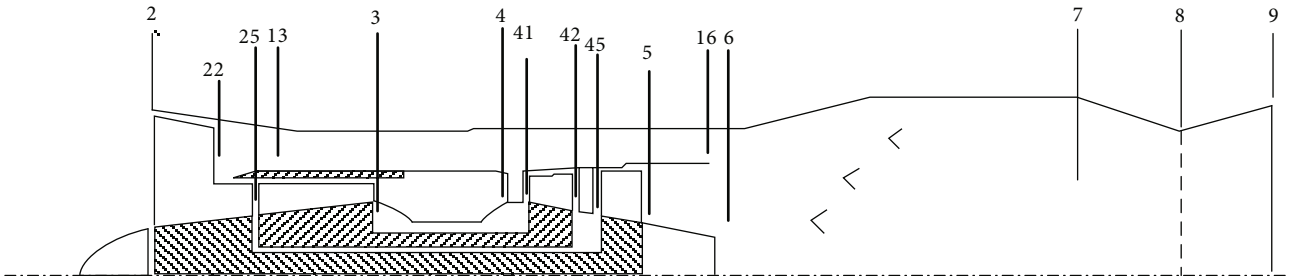

Figure 2: Turbofan engine structure diagram.

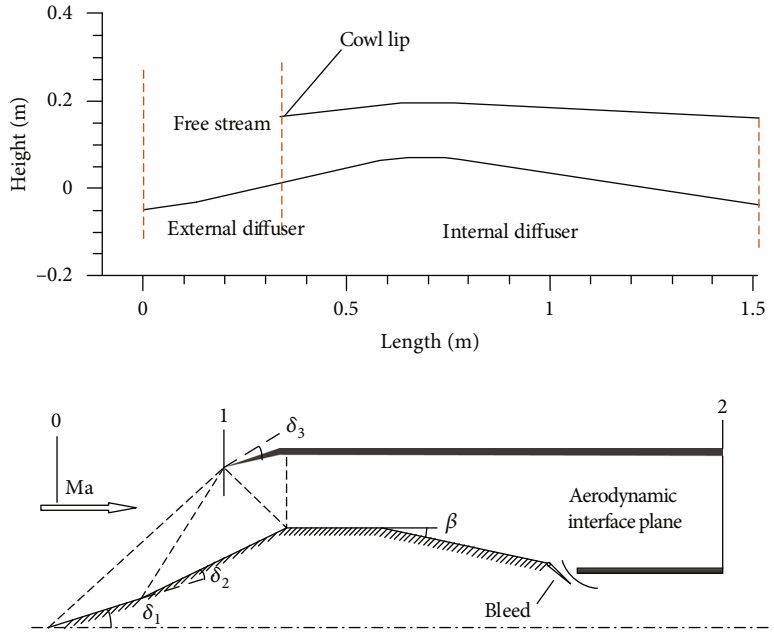

Figure 3: Inlet model.

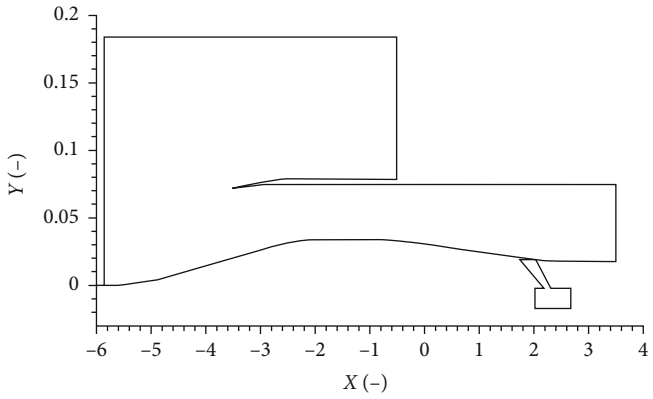

Figure 4: Computational model.

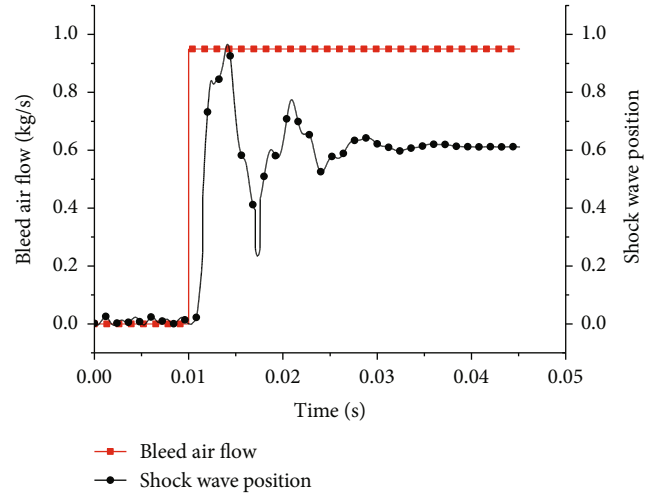

Figure 5: Shock wave position output.

At the initial time, the bleed valve is closed and the inlet flow is 17.01 kg/s. After 0.01 second, the bleed valve opens and the bleed flow reaches 0.95 kg/s, while the inlet exit flow is 16.06 kg/s. Figures 6 and 7 clearly show the change of shock wave position, and the shock wave moves to 0.6.

Furthermore, in order to facilitate the design of an inlet control system, it is necessary to establish the dynamic transfer function model of the bleeding process. Based on the

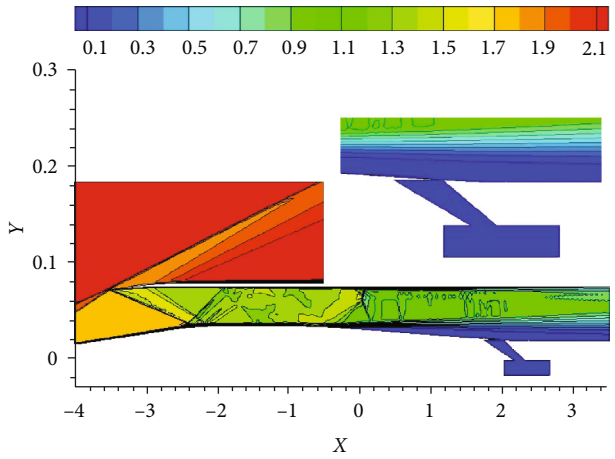

Figure 6: Mach number flow field in 0 s.

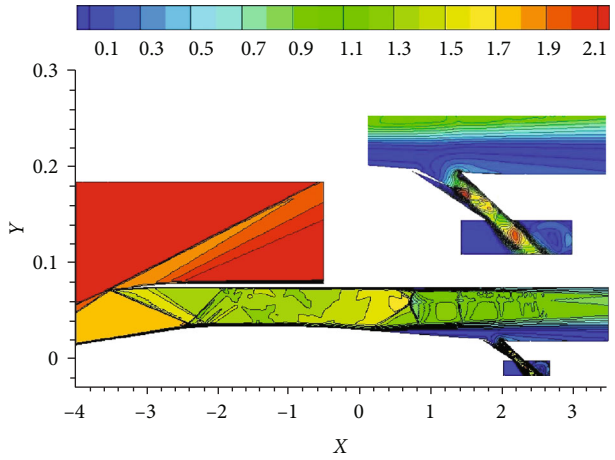

Figure 7: Mach number flow field in 0.045 s.

nonlinear least square method, the input and output curves are identified and the transfer function is obtained.

$$G_B(s) = \frac{-23.3s + 5.05 \times 10^5}{s^2 + 311.2s + 7.89 \times 10^5.} \quad (1)$$

As shown in Figure 8(a), the output of the transfer function model is basically consistent with the output of CFD calculation, which means the identification accuracy meets the requirements. In order to further verify the accuracy of the model, the mass flow of a two-dimensional CFD inlet model is increased to 1.09 kg/s, then the positive shock position curve is obtained. As shown in Figure 8(b), the transfer function model is still within acceptable accuracy range.

The inlet and engine integrated model in this paper are a component level model [16, 17]. Each component must meet the mutual restriction and follow common operating condition. The paper selects low-pressure rotor speed N_l, high-pressure rotor speed N_h, fan pressure ratio Z_f, compressor pressure ratio Z_C, high-pressure turbine equivalent mass flow $m_{41,cx}$, low-pressure turbine equivalent mass flow $m_{45,cx}$, and inlet flow coefficient φ as the initial guess values. Considering the continuity of airflow, static pressure balance, and rotor power balance, the seven equations are selected. The flow continuity residual of inlet and fan equation is shown as follows:

$$\frac{\varepsilon_1 = m_2,c - m_{21},c}{m_2,c,} \quad (2)$$

where $m_{2,c}$ is airflow of inlet, $m_{21,c}$ is airflow of fan, and ε_1 is residual error of equation.

The flow continuity residual function of a high-pressure turbine inlet is as follows:

$$\varepsilon_2 = \frac{m_{41,cx} - m_{41,c}}{m_{41,c}}, \quad (3)$$

where $m_{41,cx}$ is the high-pressure turbine initial guess flow and $m_{41,c}$ is the calculated flow.

Flow continuity residual function of a low-pressure turbine inlet is as follows:

$$\varepsilon_3 = \frac{m_{45,cx} - m_{45,c}}{m_{45,c}}, \quad (4)$$

where $m_{45,cx}$ is the low pressure turbine initial guess flow and $m_{45,c}$ is the calculated flow.

The static pressure balance residual function of the bypass outlet is as follows:

$$\varepsilon_4 = \frac{p_{16,s} - p_{6,s}}{p_{6,s}}, \quad (5)$$

where $p_{16,s}$ is the external static pressure at the outlet of bypass and $p_{6,s}$ is the internal static pressure at the outlet of the bypass.

Flow continuity residual function of the nozzle throat is as follows:

$$\varepsilon_5 = \frac{m_{8,x} - m_8}{m_8}, \quad (6)$$

where $m_{8,x}$ is the nozzle initial guess flow and m_8 is the calculated flow.

The power balance equation of a low-pressure rotor is as follows:

$$\varepsilon_6 = \frac{W_f \eta_l - W_{lt}}{W_{lt}}, \quad (7)$$

where W_{lt} is the power of a low-pressure turbine and W_f is the consumed power of fan.

The power balance equation of a high-pressure rotor is as follows:

$$\varepsilon_7 = \frac{W_c \eta_h - W_{ht}}{W_{ht}}, \quad (8)$$

where W_{ht} is the power of a high-pressure turbine and W_c is the consumed power of a compressor.

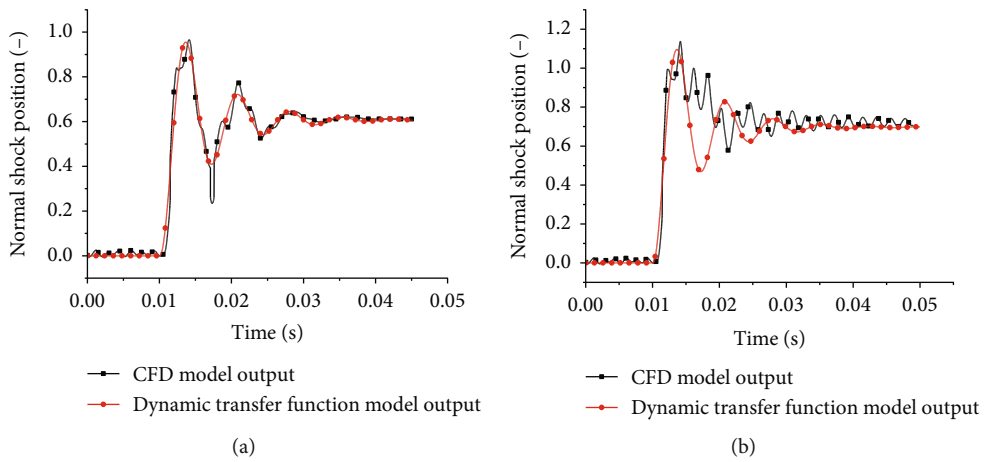

Figure 8: Output of a dynamic transfer function model.

Table 1: Relevant design parameters of the compressor blade.

Number	1	2	3	4	5	6	7	8	9
Total pressure recovery coefficient ratio	1	0.994	0.985	0.977	0.971	0.965	0.961	0.944	0.903
Normal shock position	-0.15	-0.087	0.045	0.204	0.417	0.438	0.503	0.805	0.943

The equations are solved by a Newton iteration method. While the total pressure loss of the inlet includes wall friction loss, total pressure loss of shock wave, and total pressure loss of duct after throat. The latter two account for more than 90% of the supersonic inlet's total pressure loss. When the flow condition and the shock wave position are fixed, the structure of the normal shock wave system in the supersonic inlet and the length of the expansion area after normal shock wave remain unchanged. The bleed regulation only changes a small part of the wall friction loss [18]. Therefore, the total pressure recovery coefficient, which is related to the normal shock wave position, can be approximately regarded as unchanged. The relationship between them is shown in formula (9), and correspondence is shown in Table 1.

$$\sigma = i \cdot \sigma_{\max}, \tag{9}$$

where $\sigma_{\max}$ is the total pressure recovery coefficient in critical state and i is the total pressure recovery coefficient ratio. When the position is less than -0.15, the total pressure recovery coefficient maintains the maximum value.

The calculation process of the inlet and engine integrated model is shown in Figure 9. The atmospheric turbulence model shows the upstream disturbance (ΔP_0, ΔT_0, and ΔM_0), and the engine model shows the downstream disturbance (ΔP_2). After that, the integrated model calculates the normal shock position and adopts closed-loop control by an active disturbance rejection control (ADRC) algorithm.

The block diagram of the closed-loop control loop for normal shock position is shown in Figure 10. G_A is the transfer function of the actuator. It indicates the opening and closing of the exhaust valve, which is generally controlled by a high-speed valve. In order to realize the bleed regulation, the high-speed valve produced by MOOG Company is used as the actuator and the transfer function is shown as follows:

$$G_A(s) = \frac{(s/63+1)}{(s/60+1)\left(s^2/1.29\times10^6+0.8s/1136+1\right)\left(s^2/2.26\times10^7+0.6s/4753+1\right)}. \tag{10}$$

The generalized controlled object of transfer function $G(s)$ is as follows:

$$G(s) = \frac{(s/63+1)}{(s/60+1)\left(s^2/1.29\times10^6+0.8s/1136+1\right)\left(s^2/2.26\times10^7+0.6s/4753+1\right)} * \frac{-23.3s+5.05\times10^5}{s^2+311.2s+7.89\times10^5}. \tag{11}$$

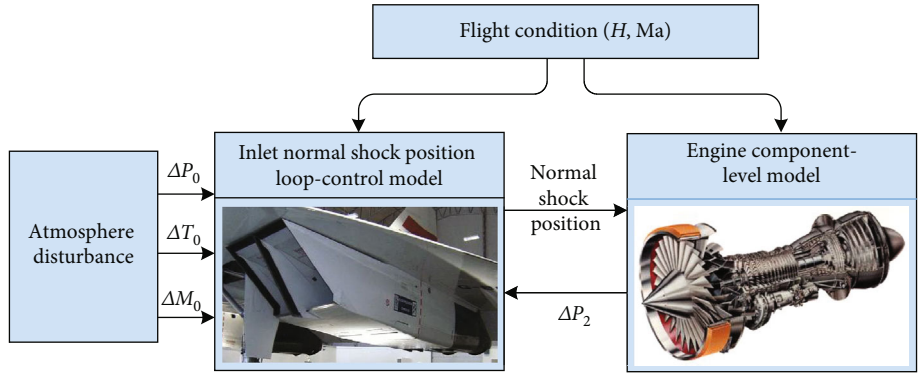

Figure 9: Inlet/engine integrated model calculation.

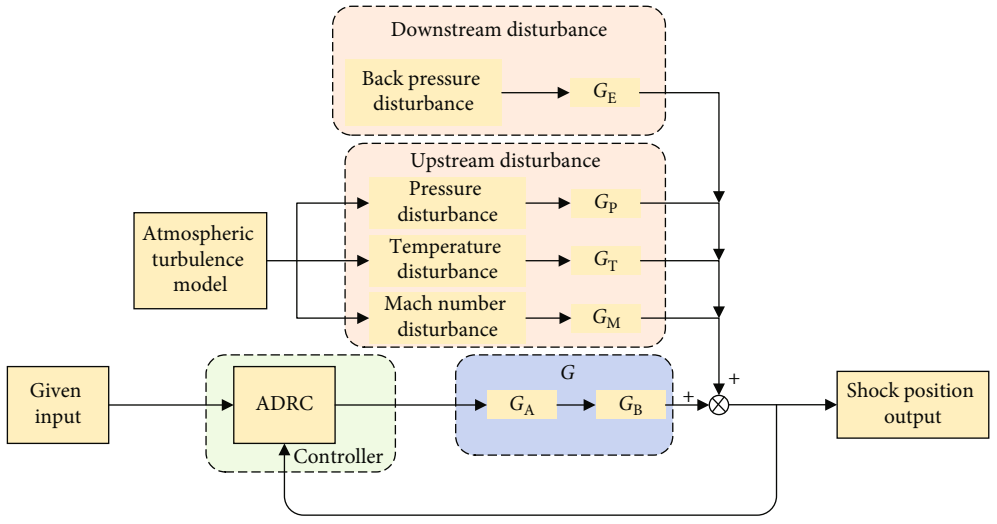

Figure 10: Normal shock position closed loop control.

The least square method is used to identify the pressure disturbance, temperature disturbance, Mach number disturbance, and back pressure disturbance. The corresponding transfer functions are as follows:

$$\begin{aligned} G_p(s) &= \frac{0.1082}{s + 187.1}, \\ G_T(s) &= \frac{4.0805s - 154.23}{s^2 + 186.2s + 2.558 \times 10^5}, \\ G_M(s) &= \frac{1630}{s + 604.5}, \\ G_E(s) &= \frac{5.326 \times 10^{-3}s - 28.28}{s^2 + 279.8s + 7.144 \times 10^5}. \end{aligned} \tag{12}$$

According to the corresponding relationship between the shock position and the total pressure recovery coefficient, the total pressure recovery coefficient in the engine model is modified. Then, the thrust and other performance of the engine are calculated.

3. Simulation of Integrated Model

The inlet model simply gives the maximum total pressure recovery coefficient under the current flight conditions. The change of engine state does not affect the inlet total pressure recovery coefficient, and this phenomenon is obviously unconventional. With the change of the inlet state, the inlet would enter into the supercritical state and the total pressure recovery coefficient would decrease. Therefore, the inlet normal shock wave and engine model are combined together. The different working conditions of inlet could be simulated, and the coupling relationship between the engine and inlet is clarified by modifying the total pressure recovery coefficient through the normal shock wave position. The pressure, temperature, velocity, and downstream disturbance of an integrated model are simulated to test the operation effect in this paper.

The verification point of pressure disturbance is $H =$ 11 km, Ma = 2.2, and PLA = 50 degrees. Figure 11 shows the simulation results of an integrated model under pressure disturbance. In the pictures, Figure 11(a) is the

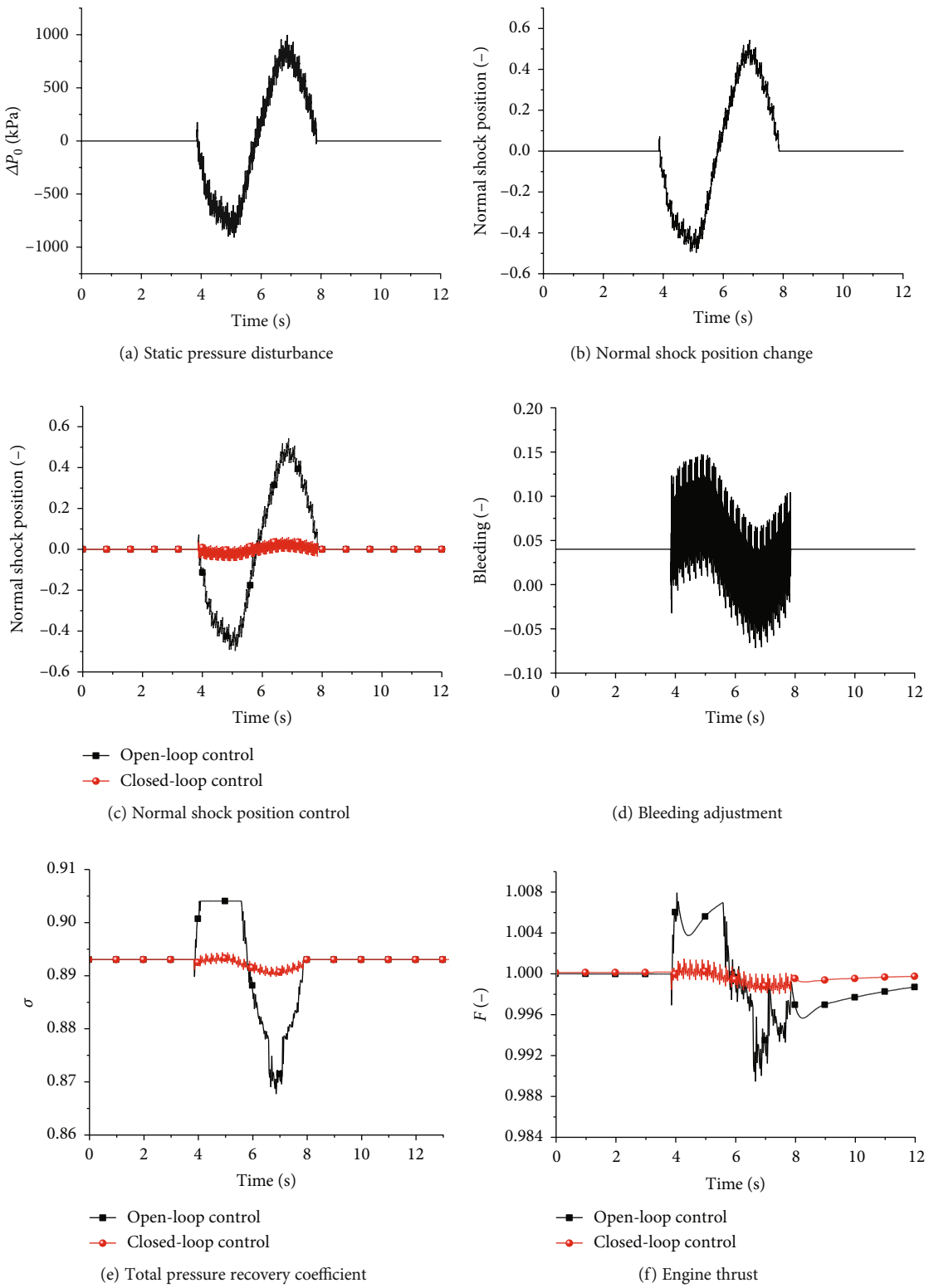

(a) Static pressure disturbance

(b) Normal shock position change

(c) Normal shock position control

(d) Bleeding adjustment

(e) Total pressure recovery coefficient

(f) Engine thrust

Figure 11: Simulation results of an integrated model under pressure disturbance.

output disturbance of a turbulence model, Figure 11(b) is the disturbance of normal shock wave position caused by a turbulence model, Figure 11(c) is the change of normal shock position in closed- and open-loop control, Figure 11(d) is the bleed flow in closed-loop control, and Figures 11(e) and 11(f) are the comparison of total pressure recovery coefficient and engine thrust. In 3.8 seconds, the inlet normal shock model exerts inflow static pressure

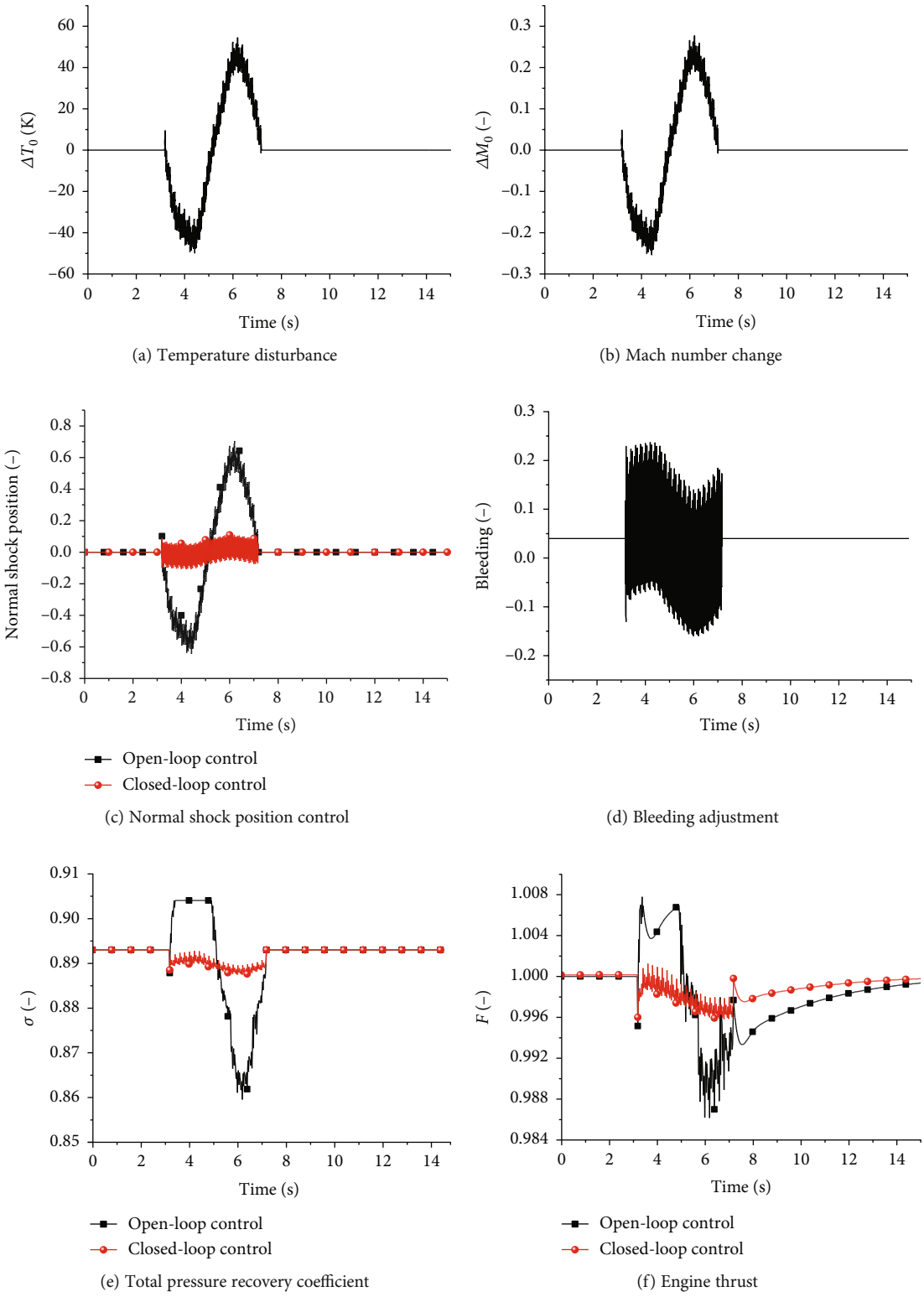

Figure 12: Simulation results of an integrated model under temperature disturbance.

disturbance (±1000 Pa), which is caused by a turbulence model. The normal shock wave position changes, and the amplitude of the fluctuation is about 0.54. When the system does not include ADRC controller, the disturbance of normal shock wave position is transmitted directly to the engine model that results in the huge change of total pressure recovery coefficient σ and thrust F. With the change of the position, σ rises to the maximum value 0.904, then drops to 0.868, and

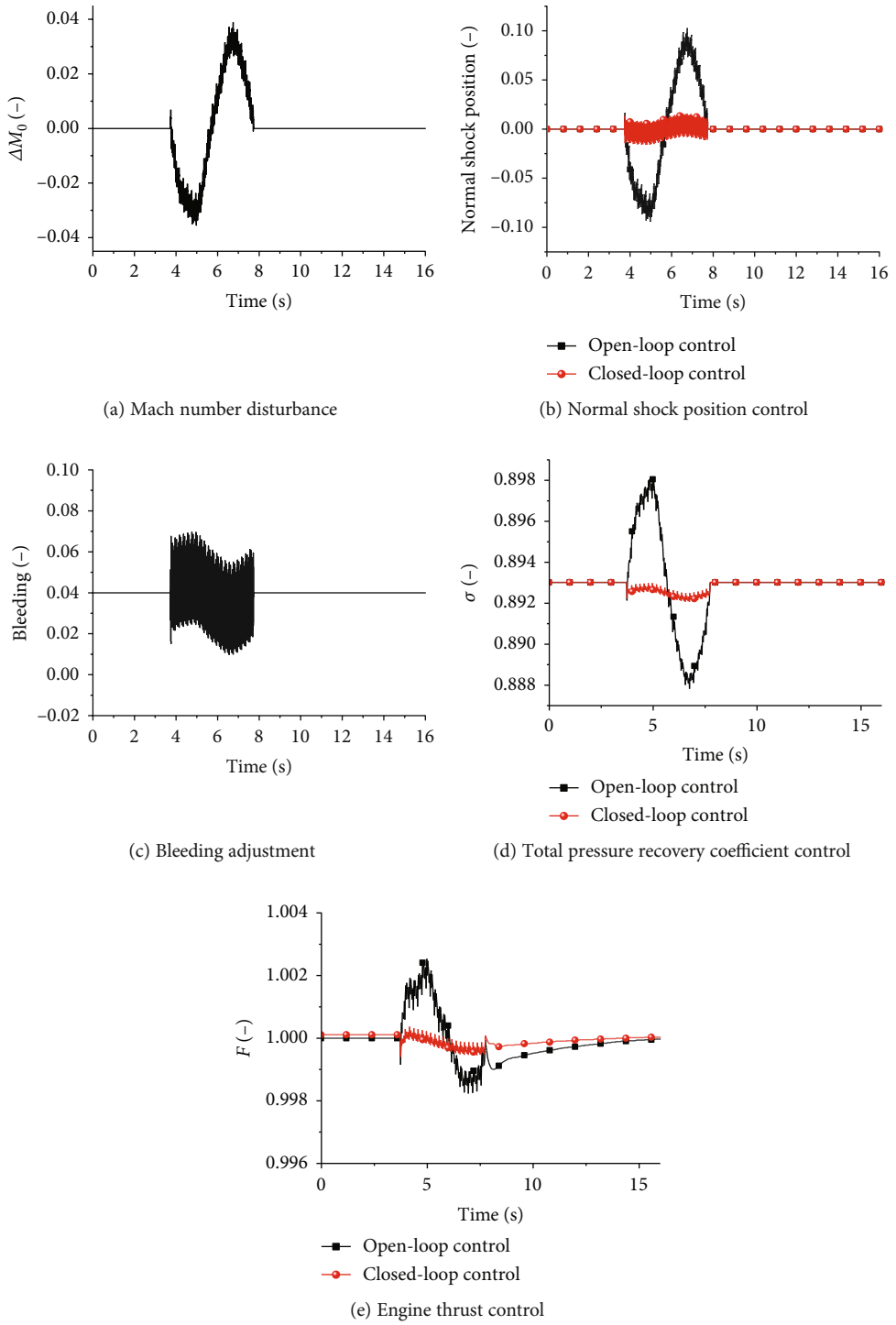

Figure 13: Simulation results of an integrated model under Mach number disturbance.

trends to be stable finally. The thrust increases as the normal shock wave position moves toward the throat and decreases when it moves to the exit of the inlet. When the normal shock wave model adopts closed-loop control, the position could set at 0 and is at the best matching point. The total pressure recovery coefficient is basically stable compared with the open-loop control, and the fluctuation is small. The engine thrust has little change and hovers around 1. In general, the closed-loop control of normal shock position can stabilize the engine working condition and reduce the influence of pressure disturbance on the engine. The bleed flow has an initial value of 0.04, and the flow can be used as the air convection in the cabin of the aircraft.

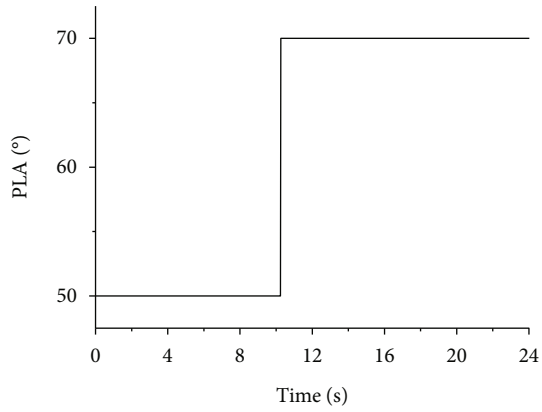

Figure 14: Change of the throttle lever angle.

In order to verify the ability of the integrated model to resist temperature disturbance, the test has been carried out. The verification point of temperature disturbance is $H = 11$ km, Ma = 2.2, and PLA = 50 degrees. Figure 12 shows the simulation results of an integrated model under temperature disturbance. In 3.2 s, the inlet normal shock wave model exerts inflow temperature disturbance (±50 K), which is caused by a turbulence model. Figure 12(a) is the output disturbance of a turbulence model. With the change of temperature, the Mach number changed. Figure 12(b) is the disturbance of the Mach number, and the disturbance is between ±0.25. Figure 12(c) is the change of normal shock wave position in closed- and open-loop control, whose amplitude is about 0.6. When the model is in closed-loop control, the position could be well stabilized at the best match point. Compared with the open-loop control, the advantage is more obvious. Because the position of the normal shock wave is fixed in the closed-loop control system, the total pressure recovery coefficient and engine thrust are relatively stable, while the amplitude of fluctuation is smaller.

Similarly, when the Mach number is disturbed, it would also affect the position of the normal shock wave. Figure 13 shows the simulation results of an integrated model under Mach number disturbance. When the Mach number changes as shown in Figure 13(a), the change of position is between ±0.25. The effect of the closed-loop control of the normal shock position is still very stable in the closed-loop control, whose change could be neglected. Figure 13(d) shows the bleed flow in closed-loop control. Compared with the open-loop control, the total pressure recovery coefficient has little change and the thrust could also be basically stabilized.

In order to verify the ability of the integrated model to resist downstream disturbance, the next test has been carried out. The verification point of temperature disturbance is $H = 11$ km, Ma = 2.2, and the throttle lever angle is changed. The engine is adjusted from the throttling state to the intermediate state and PLA has changed from 50 degrees to 70 degrees as shown in Figure 14. Figure 15 shows the simulation results of an integrated model under downstream disturbance. The increase of the throttle lever angle leads to the rise of the engine demand flow and the inlet exit back pressure. The normal shock wave position would move toward the downstream of the throat, which makes the inlet enter into the supercritical state. Figures 15(a) and 15(b) show the change of back pressure and normal shock wave position. The difference between the open-loop control and closed-loop control is that the closed-loop control stabilizes the normal shock position and the parameters of the inlet exit are basically unchanged, which makes the back pressure decrease and the disturbance of normal shock wave position gets smaller. Figure 15(c) clearly shows the effect of closed-loop control. With the closed loop of normal shock position, the position remains basically unchanged at 0. While the position with open loop moves back about 0.9. Figure 15(d) is the change of bleeding in closed-loop control. It can be seen from Figure 15(e) that the total pressure recovery coefficient could also maintain at the optimal integrated point. In Figure 15(f), the engine output thrust increases by 0.05 compared with the open-loop control when the throttle lever angle is set to 70 degrees.

The integrated model could accurately describe the performance of the engine when the normal shock wave position changes. Meanwhile, the model verifies that the closed-loop control is more effective. In particular, when the upstream and downstream are disturbed, the position could always be stable at the optimal matching point and the engine thrust performance is optimal at this moment.

Additional calculations show that the inlet closed-loop control of inlet normal shock wave position obtains good robustness and could be controlled stably at different working points ($M = 2.2$ and $M = 2.3$). The disturbance is shown in Figures 16(a) and 16(b), which is the disturbance of normal shock position. Figure 16(c) is the comparison of normal shock position in closed- and open-loop control. Figure 16(d) is the bleed flow in closed-loop control. Figures 16(e) and 16(f) are the comparison of total pressure recovery coefficient and engine thrust.

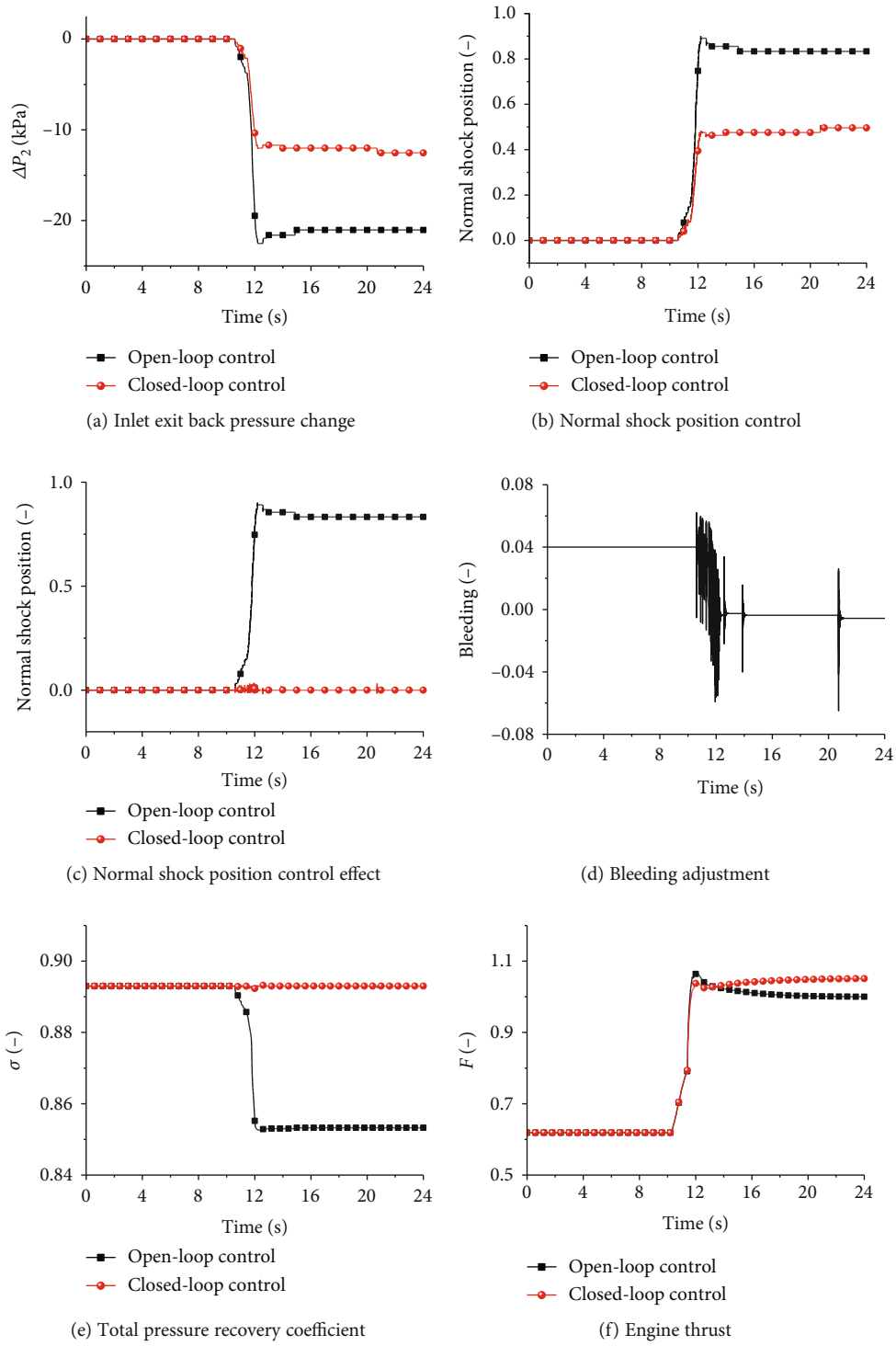

FIGURE 15: Simulation results of an integrated model under downstream disturbance.

During the closed-loop control process, the inlet and engine could be kept at the optimal matching point.

4. Conclusions

In this paper, the effects of bleed flow on the dynamic and static characteristic of normal shock wave position were investigated based on the supersonic inlet two-dimensional CFD model. The transfer function is identified, and the inlet and engine integrated model are established based on the closed-loop control of inlet normal shock wave position. The integrated model is verified by disturbance rejection simulation. The results show that the closed-loop control of inlet normal shock wave position

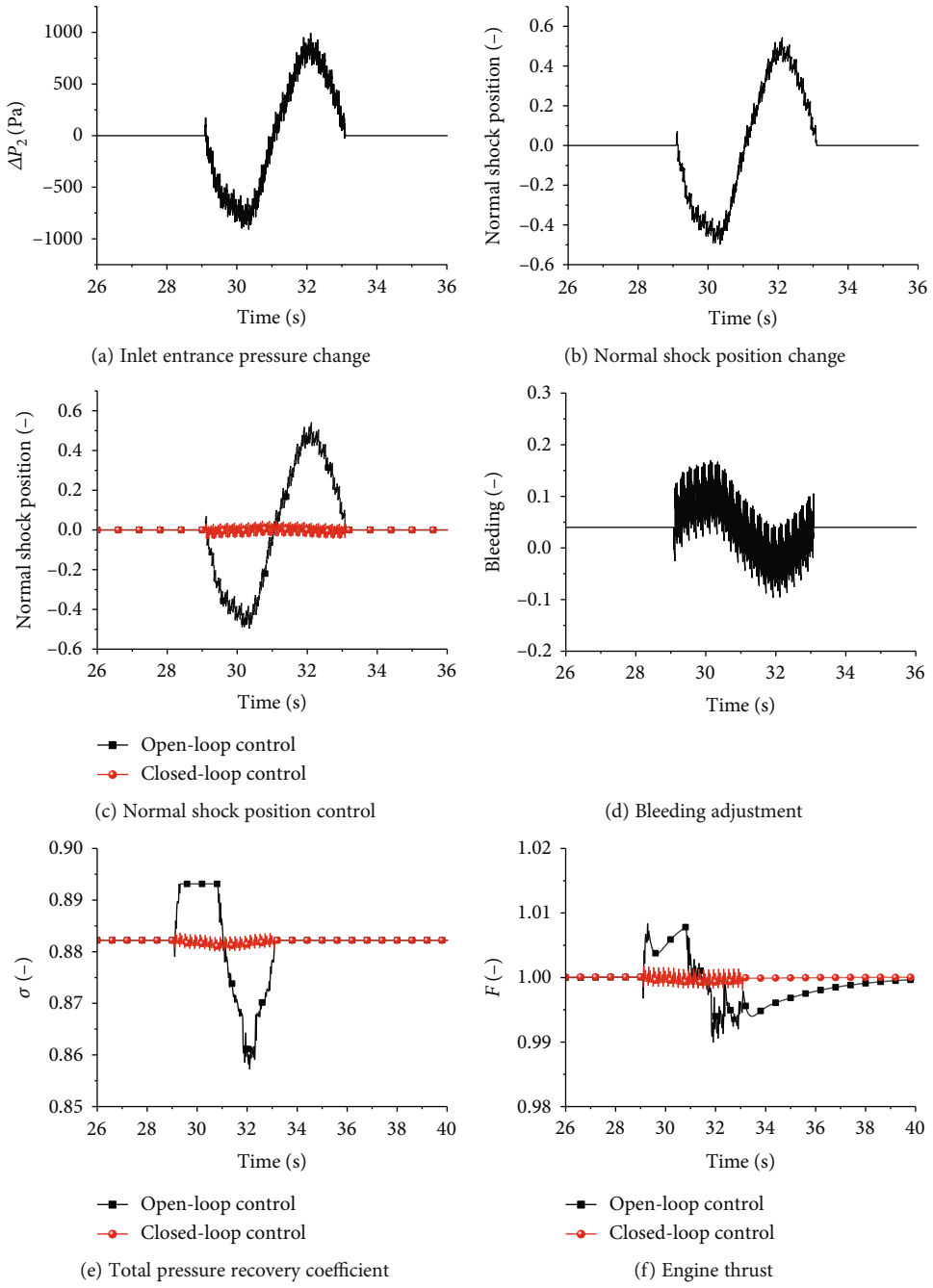

Figure 16: Simulation results of different operating points.

is effective under the action of upstream and downstream disturbances. Compared with the open-loop control, the amplitude of engine thrust is smaller in closed-loop control.

Nomenclature

C_{bp}: The coefficient of bleed drag
A_{bp}: The bleed area
HPC: High-pressure compressor
F_{in}: Installed engine thrust
N_l: Low-pressure corrected rotational speed
N_h: High-pressure corrected rotational speed
W_{fb}: Fuel mass flow rate
$m_{2,c}$: Airflow of inlet
$m_{21,c}$: Airflow of fan
$m_{41,cx}$: The high-pressure turbine initial guess flow
$m_{41,c}$: The calculated flow
$m_{45,cx}$: The low-pressure turbine initial guess flow
$m_{45,c}$: The calculated flow
$m_{16,s}$: The external static pressure at the outlet of bypass
$m_{6,s}$: The internal static pressure at the outlet of bypass
$m_{8,x}$: The total pressure calculated by flow

m_8: The total pressure calculated by inflow pressure
W_f: The consumed power of fan
W_{lt}: The power of low-pressure turbine
W_c: The consumed power of compressor
W_{ht}: The power of high-pressure turbine
H: Flight height
Ma: Mach number
ε: Residual error of equation
σ: Total pressure recovery coefficient
η_l: Fan coefficient
η_h: Compressor coefficient
PLA: Power level angle.

Data Availability

The data used to support the findings of this study are available from the corresponding author upon request.

Conflicts of Interest

The authors declare that they have no conflicts of interest.

Acknowledgments

This study is supported by the National Natural Science Foundation of China (No. 51576096).

References

[1] K. Shahrokhi and M. Davis Jr., "Application of a modified dynamic compression system model to a low aspect ratio fan-effects of inlet distortion," in *33rd Aerospace Sciences Meeting and Exhibit*, p. 301, Reno, NV, USA, January 1995.

[2] R. T. Biedron and T. C. Adamson Jr., "Unsteady flow in a supercritical supersonic diffuser," *AIAA Journal*, vol. 26, no. 11, pp. 1336–1345, 1988.

[3] M. Chen, J. Zhang, and H. Tang, "Performance analysis of a three-stream adaptive cycle engine during throttling," *International Journal of Aerospace Engineering*, vol. 2018, Article ID 9237907, 16 pages, 2018.

[4] J. Connolly, G. Kopasakis, D. Paxson, E. Stuber, and K. Woolwine, "Nonlinear dynamic modeling and controls development for supersonic propulsion system research," in *47th AIAA/ASME/SAE/ASEE Joint Propulsion Conference & Exhibit*, p. 5635, San Diego, CA, USA, July-August 2011.

[5] G. Kopasakis, J. Connolly, D. Paxson, and K. Woolwine, "Quasi 1d modeling of mixed compression supersonic inlets," in *50th AIAA Aerospace Sciences Meeting including the New Horizons Forum and Aerospace Exposition*, p. 775, Nashville, Tennessee, January 2012.

[6] J. Connolly, G. Kopasakis, and K. Lemon, "Turbofan volume dynamics model for investigations of aero-propulso-servo-elastic effects in a supersonic commercial transport," in *45th AIAA/ASME/SAE/ASEE Joint Propulsion Conference & Exhibit*, p. 4802, Denver, Colorado, August 2010.

[7] J. Pilet, J. L. Lecordix, N. Garcia-Rosa, R. Barènes, and G. Lavergne, "Towards a fully coupled component zooming approach in engine performance simulation," in *ASME 2011 Turbo Expo: Turbine Technical Conference and Exposition*, pp. 287–299, Vancouver, British Columbia, Canada, January 2011.

[8] H. Huttenlocher, R. Steele, C. Thomson, and B. Mellinger, "A critique of the F-14A air inlet control system-from development to production status," in *10th Propulsion Conference*, p. 1060, San Diego, CA, USA, October 1974.

[9] D. B. Le, C. P. Goyne, and R. H. Krauss, "Shock train leading-edge detection in a dual-mode scramjet," *Journal of Propulsion and Power*, vol. 24, no. 5, pp. 1035–1041, 2008.

[10] J. Hutzel, D. Decker, R. Cobb, P. King, M. Veth, and J. Donbar, "Scramjet isolator shock train location techniques," in *49th AIAA Aerospace Sciences Meeting including the New Horizons Forum and Aerospace Exposition*, p. 402, Orlando, Florida, January 2011.

[11] J. Donbar, "Shock train position control in an axisymmetric scramjet combustor flowpath," in *48th AIAA/ASME/SAE/ASEE Joint Propulsion Conference & Exhibit*, p. 4145, Atlanta, GA, USA, July-August 2012.

[12] H. Chen, F. Sun, H. Zhang, and W. Luo, "A study on the stall detection of an axial compressor through pressure analysis," *Applied Sciences*, vol. 7, no. 8, p. 766, 2017.

[13] T. Jones, "Evaluation of the X-43A scramjet engine controller performance by Monte Carlo technique," in *39th AIAA/ASME/SAE/ASEE Joint Propulsion Conference and Exhibit*, p. 5192, Huntsville, AL, USA, July 2003.

[14] G. Kopasakis, "Atmospheric turbulence modeling for aerospace vehicles: fractional order fit," U.S. Patent 8, 938, 377[P], 2015.

[15] G. D. Nastrom and K. S. Gage, "A climatology of atmospheric wavenumber spectra of wind and temperature observed by commercial aircraft," *Journal of the Atmospheric Sciences*, vol. 42, no. 9, pp. 950–960, 1985.

[16] Y. Zhang, H. J. Tan, S. Sun, and C. Y. Rao, "Control of cowl shock/boundary-layer interaction in hypersonic inlets by bump," *AIAA Journal*, vol. 53, no. 11, pp. 3492–3496, 2015.

[17] S. Farokhi, *Aircraft Propulsion*, John Wiley & Sons, 2014.

[18] K. Lee, B. Lee, S. Kang, S. Yang, and D. Lee, "Inlet distortion test with gas turbine engine in the altitude engine test facility," in *27th AIAA Aerodynamic Measurement Technology and Ground Testing Conference*, p. 4337, Chicago, IL, USA, June 2010.